Proc. Natl. Acad. Sci. USA
Vol. 92, pp. 10762–10766, November 1995
Biochemistry

Crystal structure of *Pseudomonas aeruginosa* catabolic ornithine transcarbamoylase at 3.0-Å resolution: A different oligomeric organization in the transcarbamoylase family

(allostery/oligomeric enzymes/noncrystallographic symmetry/phase extension)

VINCENT VILLERET*†‡, CATHERINE TRICOT§, VICTOR STALON§, AND OTTO DIDEBERG*¶

*Laboratoire de Cristallographie Macromoléculaire, Institut de Biologie Structurale Jean-Pierre Ebel (Commissariat à l'Energie Atomique-Centre National de la Recherche Scientifique), 41 avenue des Martyrs, 38027 Grenoble Cedex 1, France; †Institut de Physique, Cristallographie, B5, Université de Liège, Sart-Tilman, 4000 Liège, Belgium; and §Laboratoire de Microbiologie, Université Libre de Bruxelles, avenue E. Gryson, 1, B-1070 Brussels, Belgium

Communicated by William N. Lipscomb, Harvard University, Cambridge, MA, August 7, 1995

ABSTRACT **The crystal structure of the Glu-105 → Gly mutant of catabolic ornithine transcarbamoylase (OTCase; carbamoyl phosphate + L-ornithine = orthophosphate + L-citrulline, EC 2.1.3.3) from *Pseudomonas aeruginosa* has been determined at 3.0-Å resolution. This mutant is blocked in the active R (relaxed) state. The structure was solved by the molecular replacement method, starting from a crude molecular model built from a trimer of the catalytic subunit of another transcarbamoylase, the extensively studied aspartate transcarbamoylase (ATCase) from *Escherichia coli*. This model was used to generate initial low-resolution phases at 8-Å resolution, which were extended to 3-Å by noncrystallographic symmetry averaging. Four phase extensions were required to obtain an electron density map of very high quality from which the final model was built. The structure, including 4020 residues, has been refined to 3-Å, and the current crystallographic *R* value is 0.216. No solvent molecules have been added to the model. The catabolic OTCase is a dodecamer composed of four trimers organized in a tetrahedral manner. Each monomer is composed of two domains. The carbamoyl phosphate binding domain shows a strong structural homology with the equivalent ATCase part. In contrast, the other domain, mainly implicated in the binding of the second substrate (ornithine for OTCase and aspartate for ATCase) is poorly conserved. The quaternary structures of these two allosteric transcarbamoylases are quite divergent: the *E. coli* ATCase has pseudo-32 point-group symmetry, with six catalytic and six regulatory chains; the catabolic OTCase has 23 point-group symmetry and only catalytic chains. However, both enzymes display homotropic and heterotropic cooperativity.**

Pseudomonas aeruginosa is an arginine prototrophic organism that possesses two distinct ornithine transcarbamoylases (OTCase; carbamoyl phosphate + L-ornithine = orthophosphate + L-citrulline, EC 2.1.3.3) (1, 2). An anabolic OTCase encoded by the *argF* gene is involved in the arginine biosynthesis pathway and catalyzes *in vivo* the thermodynamically favored formation of citrulline and phosphate from ornithine and carbamoyl phosphate. The anabolic enzyme is a trimer of identical 34-kDa subunits (3) and displays Michaelis–Menten kinetics (3, 4). *P. aeruginosa* possesses a second OTCase, encoded by the *arcB* gene, which is involved in the anaerobically inducible arginine deiminase pathway and promotes *in vivo* the phosphorolysis of citrulline, the reverse reaction of the biosynthetic one, yielding ornithine and carbamoyl phosphate (1, 2, 5, 6). This catabolic OTCase does not carry out the biosynthetic reaction because of a poor affinity and a marked cooperativity for carbamoyl phosphate (7). Moreover, the enzyme is heterotropically activated by nucleoside monophosphates (AMP, GMP, CMP, UMP) and is inhibited by some polyamines such as spermidine and putrescine (8). The catabolic OTCase is an oligomeric enzyme of high molecular weight (456 kDa), and preliminary x-ray diffraction studies suggested a dodecameric structure made of 38-kDa subunits (9). Despite different quaternary organizations, the primary structure of both anabolic and catabolic OTCases is quite similar, and the catabolic OTCase of *P. aeruginosa* is even closer to the anabolic OTCase of *Escherichia coli* than the anabolic enzyme of *P. aeruginosa* (3, 10). A mutant form of the catabolic OTCase obtained by *in vivo* mutagenesis and in which glutamate-105 is replaced by a glycine is able to perform the anabolic reaction *in vivo*. This mutant is devoid of homotropic cooperativity, while a Hill coefficient of 4.3 is observed for the wild-type enzyme. Therefore, the Glu-105 → Gly mutant is blocked in the active R (relaxed) form (7, 8, 11). Structural knowledge of the T (tight) and R forms of the enzyme is required to investigate the complex allosteric behavior of this catabolic enzyme. Furthermore, a large number of studies have been pursued over the past 25 years on the allosteric aspartate transcarbamoylase (ATCase) from *E. coli* (12), which catalyzes the carbamoylation of aspartate to form carbamoyl L-aspartate. Structural studies of the catabolic OTCase should stimulate new insights in the entire field of transcarbamoylases. We report here the 3.0-Å crystal structure of the Glu-105 → Gly mutant of the catabolic OTCase from *P. aeruginosa* and its structural comparison to the well-known ATCase from *E. coli*.‖ These enzymes illustrate the great structural diversity found among the transcarbamoylase family.

MATERIALS AND METHODS

Crystallizations, Data Collection, and Processing. Preliminary crystallization trials have been described (9). Both the native enzyme and the Glu-105 → Gly mutant were available at the beginning of this study and were included in the experiments. Crystallizations were performed by the hanging-drop technique at 21°C. The best crystals were obtained with the Glu-105 → Gly mutant by vapor diffusion against a reservoir solution containing 50 mM Hepes (pH 7.0), 50% (wt/vol) ammonium sulfate, 1 mM dithiothreitol, and 1 mM EDTA. The protein (24 mg/ml, in the same buffer) was mixed 1:1 with this solution. Routinely, plate-shaped crystals were

The publication costs of this article were defrayed in part by page charge payment. This article must therefore be hereby marked "*advertisement*" in accordance with 18 U.S.C. §1734 solely to indicate this fact.

Abbreviations: OTCase, ornithine transcarbamoylase; ATCase, aspartate transcarbamoylase; T, tight; R, relaxed.

‡Present address: Gibbs Chemical Laboratory, Harvard University, 12 Oxford Street, Cambridge, MA 02138.
¶To whom reprint requests should be addressed.

‖The atomic coordinates have been deposited in the Protein Data Bank, Chemistry Department, Brookhaven National Laboratory, Upton, NY 11973 (reference no. 1ORT).

formed in about 3–5 days. The biggest crystals reached dimensions of 1.2 × 0.5 × 0.25 mm^3 and diffracted at least to 3.0-Å resolution.

Data were collected with a FAST (Enraf Nonius) television area detector using CuKα radiation produced by an Elliott GX21 rotating anode generator equipped with a graphite monochromator and running at 40 mA and 90 kV. Rotation frames of 0.12° around an arbitrary axis were collected with an exposure time of 90 s per frame. Data collection and processing were performed with the program MADNES (13). Three batches of reflections covering a total of 220° of data were scaled and reduced with ROTAVATA/AGROVATA programs of the CCP4 package (14). The space group is $P1$, with cell dimensions a = 110.36 Å, b = 126.42 Å, c = 134.54 Å, α = 85.07°, β = 59.24°, and γ = 111.97°. A total of 116,334 observations were recorded for 92,630 unique reflections. The reduced data are 85% complete between 30 and 3 Å with a R_{merge} value of 0.05. The protein content parameter V_m (15) is ≈3.07 $Å^3$/dalton for one oligomer consisting of 12 monomers (total of 456 kDa) per cell. Four threefold and three twofold noncrystallographic symmetry axes were first identified with MERLOT (16) and X-PLOR (17) and further refined by using the locked rotation function (program GLRF, ref. 18). The angles between these axes were close to the theoretical values calculated for a 23 point-group symmetry (3–3: 70.52°; 3–2: 54.73°; 2–2: 90°). This hypothesis was confirmed with the locked rotation function, in which the local symmetry was imposed during the self-rotation search. The results were unambigous, with the first peak having a value of 11.0 σ above mean (σ = standard deviations). The oligomer has a 23 point-group symmetry and is basically made of four trimers organized in a tetrahedral manner. No axis diverges from the exact 23 symmetry by more than 0.1° at 3-Å resolution. One twofold axis of the particle is nearly parallel to the crystallographic a axis. All triclinic crystals obtained in the conditions described above were poorly isomorphous; this lack of isomorphism and the difficulty to obtain heavy atom derivatives in preliminary experiments suggested another phasing method based mainly on the use of the high noncrystallographic symmetry of our crystals.

Structure Determination. The catabolic OTCase belongs to the transcarbamoylase family, in which the *E. coli* ATCase has been extensively studied by crystallography (12). Two domains are identified in the monomer of these enzymes: the polar domain is mainly involved in the binding of carbamoyl phosphate, the common substrate for both enzymes; the equatorial domain is involved in the binding of the second substrate, ornithine for OTCase or aspartate for ATCase. The sequence identity between OTCase and ATCase is ≈30% for the polar domain but falls under 15% for the equatorial domain. The simplest functional architecture for most ornithine, aspartate, and putrescine carbamoyltransferases is a catalytically active trimer, even though these enzymes may possess a more complex quaternary structure: the native ATCase holoenzyme of *E. coli* has ≈32 point-group symmetry and is composed of two catalytic trimers linked by three regulatory dimers. When one keeps in mind the weak homology between sequences of OTCase and ATCase and their different quaternary organizations, it appeared as a challenging problem to determine our structure without heavy-atom derivatives, because only 1/24th of the dodecameric OTCase (the carbamoyl phosphate binding domain) was available as a reliable model. Classical molecular replacement methods could not be applied in this case. The strategy developed to solve the structure is based in part on the procedure used in the structure determination of the Mengo virus (20, 21) and the foot-and-mouth-disease virus (22). With the hypothesis that catabolic OTCase shows a trimeric organization similar to ATCase, a low-resolution molecular model was generated starting from the crude homologous trimeric catalytic subunit of this enzyme. Potential orientations of the trimer in the asymmetric unit were investigated with X-PLOR, GLRF, and AMORE (23) programs. Trials using X-PLOR and GLRF failed to find correct orientations, even at low resolution. Despite a lack of clear contrast between the values of the rotation function, AMORE allowed selection of potential orientations that were consistent with the expected 23 point-group symmetry. The 12 solutions that respect the 23 point-group symmetry were found within the first 17 peaks of the search procedure. The complete dodecameric model was built by testing all possibilities to assemble four oriented ATCase trimers into a compact 23-oligomeric structure. For one trimer orientation, two types of dodecameric models are possible: one where the concave face of the trimer is facing inwards and the other where it is facing outwards. For each solution the models with various compactness were generated by applying different translations along the local threefold axes. The best solution was selected on the basis of its correlation coefficient and crystal packing considerations. For phasing, the crude oligomeric particle could only be used at low resolution; the correlation coefficient was 0.42 between 15 and 8 Å, with no significant correlation observed at higher resolution. Consequently, an initial low-resolution phase set was generated between 15 and 8 Å. From this starting point, noncrystallographic symmetry averaging, solvent flattening, and careful phase extension from 8-Å to 3-Å resolution were carried out by using the DEMON package (24). Despite reasonable extension statistics (average R factor of 20.3% for all of the data between 30 and 3.0 Å), a visual inspection of this first electron density map was disappointing. We chose at this point to analyze our electron density maps at lower resolution, with the hope that some information could be used in these maps to improve the initial model. In the first map, at 6-Å resolution, a shift between the averaged density map and two α-helices of the initial model was clearly visible in the ornithine binding domain, at the periphery of the oligomer, affecting directly the molecular envelope. These secondary structures were repositioned in the density. The new model showed a better correlation (0.54) between 15- and 6-Å resolution and was used to recalculate initial phases and a more accurate envelope. Another phase extension was carried out from 6-Å to 3-Å resolution. The second density map at 3-Å resolution was again of poor quality. However, an analysis of this map at 6-Å resolution allowed us to fit precisely all of the α-helices in the electron density, except one α-helix that was truncated by the molecular envelope.

Progress in the structure determination was shown in the correlation coefficient, which was improved at 5-Å resolution. Nevertheless, no clear density was found for the two β-pleated sheets. A third phase extension was carried out from 5-Å to 4-Å resolution, starting from this better phase set and a more precise envelope. This new map at 4-Å resolution was obviously of better quality, allowing us to locate the two β-pleated sheets. A last extension was carried out to 3.0-Å resolution, starting from 4-Å resolution. This extension yielded an averaged electron density map of very high quality. The final average R factor and correlation coefficient are 15.5% and 0.95, respectively, for all data between 30.0 and 3.0 Å. This electron density map allowed us to trace an unambigous chain for the whole structure by using TURBO-FRODO (25). Since the starting phases used for phase extension were obtained from a polyalanine model, the observation in this map of most of the side chains clearly indicates the correctness of the structure. The structure has been refined with X-PLOR (running on a Hewlett–Packard 750 workstation). Strict noncrystallographic symmetry was applied during the whole refinement process. The initial model built in the averaged electron density showed an R factor of 48%. Two hundred cycles of least-squares minimization lowered the R factor to 34%. A simulated annealing refinement according to the slow-cooling protocol of X-PLOR was then carried out and produced a model with R = 26%. At that time some manual corrections were

applied. Conventional atomic positions and grouped B-factor refinements yielded a model with $R = 21.6\%$ in strict noncrystallographic symmetry without water molecules and thus yielded no model for solvent structure. The root-mean-square deviations from ideal values are 0.015 Å for bond lengths and 4.01° for bond angles.

RESULTS AND DISCUSSION

Monomer Structure. The OTCase monomer has 335 residues and is composed of two domains: the carbamoyl phosphate domain (or polar domain; residues 1–150) and the ornithine binding domain (or equatorial domain; residues 151–283). An α helix is present at the C terminus (residues 284–335) and is part of the two domains. The N- and C-terminal residues are observed in the averaged electron density map and are located in the polar domain close to each other. Each domain is made up of a β-sheet of five parallel strands surrounded by α-helices: six in the polar domain and eight in the equatorial domain. The topology of these two domains is α/β, as observed in the ATCase monomer. The secondary structures are defined in Fig. 1 for both OTCase and ATCase. If we compare the polar domains of these two transcarbamoylases, the main differences are found in helix H1, which shows an additional turn at its carboxyl end in the OTCase. The root-mean-square deviation calculated between α-carbon atoms (without coils and the end of helix H1) is 1.2 Å. The equatorial domains are poorly conserved, with root-mean-square deviations ranging from 0.3 Å for the B6 strand to 5.1 Å for helix H10. Helix H7 also has an additional turn at its carboxyl end in OTCase, and a new helix is present between strand B10 and helix H11. Two different conformations are observed for the ATCase monomer between the T and R allosteric states: an effective domain closure occurs upon binding of *N*-phosphonoacetyl L-aspartate (PALA), a bisubstrate analogue that induces the allosteric transition (26–28). This domain closure involves a rotation of the equatorial domain of 5° relative to the polar domain. The OTCase monomer is in a more opened form than the two conformations observed for the ATCase monomer, approximately 12° and 16° relative to the T and R forms, respectively (Fig. 2). This more opened form probably allows ornithine binding in the active site.

Trimer Structure. The trimeric organizations of both OTCase and ATCase are rather similar, with an approximate form of a disk with a radius and thickness of 55 Å. The active sites

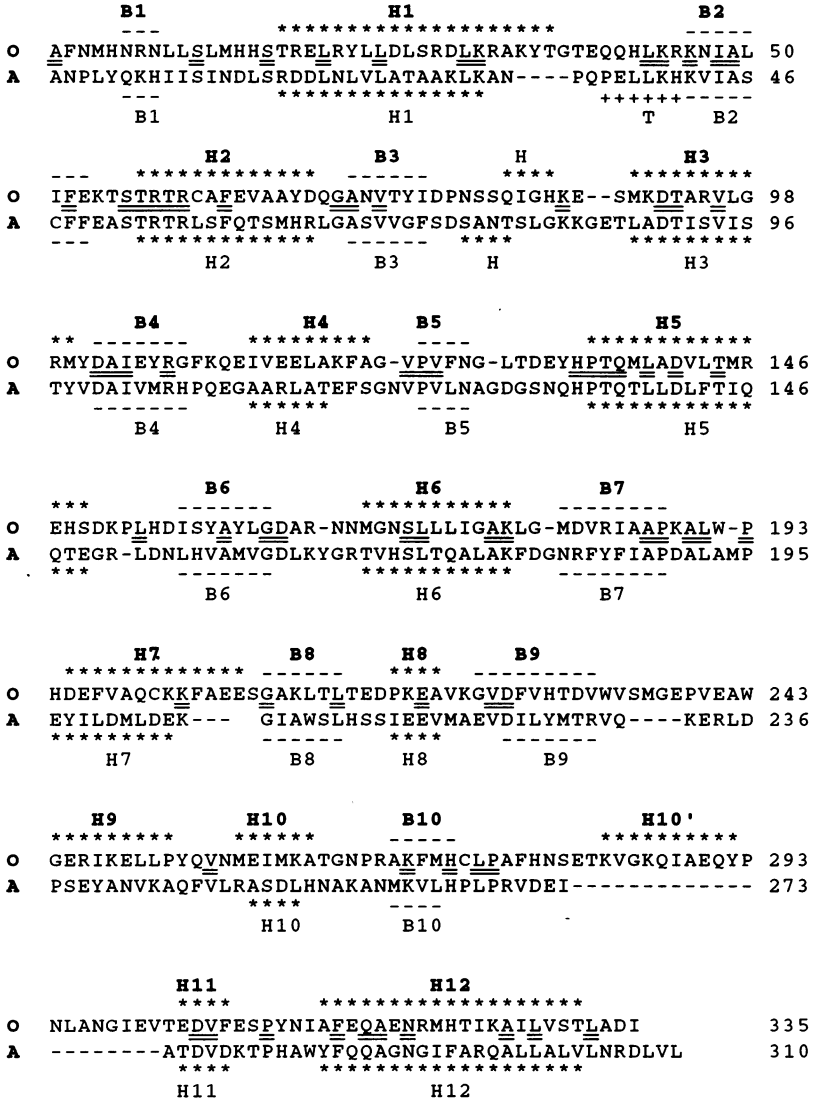

FIG. 1. Alignment of *P. aeruginosa* catabolic OTCase (O) and *E. coli* ATCase (A) sequences. ATCase secondary structures are those defined by Ke *et al.* (26), and OTCase secondary structures are defined from the ϕ and ψ dihedral angles of the main chain. Regions of α-helices are indicated by an asterisk, and regions of β-strands are indicated with a broken line. Residues strictly conserved between the two sequences are indicated with a double line.

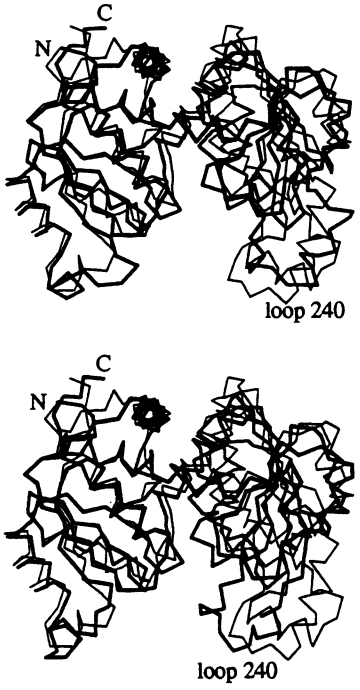

FIG. 2. (*Upper*) View of the monomer from *P. aeruginosa* catabolic OTCase (thin line) superimposed onto the T state form of the catalytic monomer from *E. coli* ATCase. (*Lower*) View of the monomer from *P. aeruginosa* catabolic OTCase (thin line) superimposed onto the R state form of the catalytic monomer from *E. coli* ATCase.

are found on the concave face of the trimers. Interfaces between monomers involve mainly residues from the polar domains, which are well conserved between the two transcarbamoylases. These residues belong to helices H2, H12, and B10–H10′ from one monomer and B2, B3–H3, and H3 from another monomer. Three salt bridges are identified at all of the interfaces between two monomers inside each trimer: between Arg-58 and Glu-88, Glu-307 and Arg-95, and Glu-318 and Arg-99. The salt bridge observed between Arg-58 and Glu-88 is also found in the R state ATCase (Arg-54–Glu-86) (29) and probably stabilizes the B3–H3 loop in its active conformation in the two enzymes.

Dodecamer Structure. The oligomer consists of four trimers and has the 23 point-group symmetry. The structure can be shown as a tetrahedron of which each face is constituted by a trimer. The four threefold symmetry axes are perpendicular to the faces in their center and the three twofold axes pass through the middles of opposite edges. The convex faces of the trimers are oriented towards the inner side of the particle. The greatest dimension of the dodecamer is 130 Å when viewed along a twofold or a threefold symmetry axis (Fig. 3). An inner cavity of ≈20-Å diameter is present in the structure.

Each monomer is involved in two different interfaces between trimers in the dodecamer. The first interface is located around a twofold symmetry axis and involves mainly the N- and C-terminal residues. The second interface is located around a threefold symmetry axis (at one edge of the dodecamer) and involves residues from helices H1 and H5. Three H1 and H5 helices from three monomers belonging to different trimers are present in this region. Twelve arginines from these secondary structures are found in the interface: three arginines from each H1 helix (Arg-21, Arg-28, and Arg-32) and Arg-146 from each H5 helix. These arginines are organized into four rings around the threefold symmetry axis. One sulfate ion is clearly defined in the averaged electron density map on the threefold symmetry axes, in the middle of the four rings made by these arginines (Fig. 4). None of these four residues is

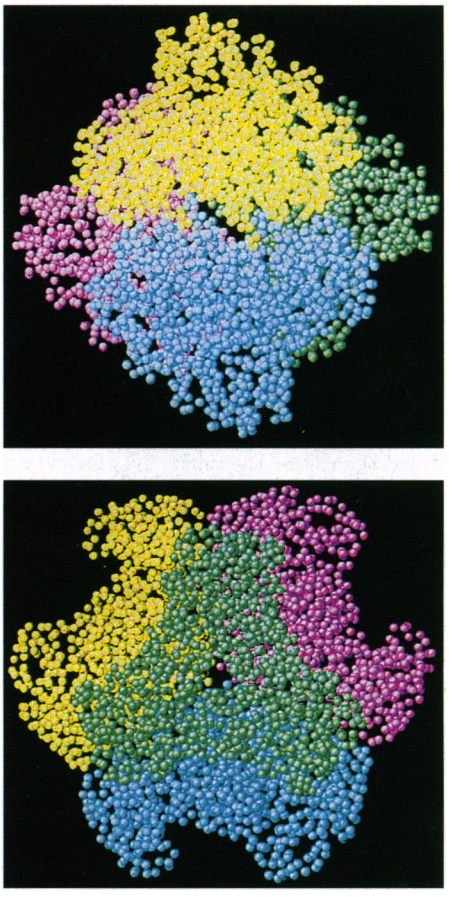

FIG. 3. (*Upper*) Corey–Pauling–Koltun (CPK) representation of the *P. aeruginosa* catabolic OTCase viewed along a twofold axis. Each trimer is represented by a different color, and only the α-carbons were used to generate the picture. (*Lower*) CPK representation of the *P. aeruginosa* catabolic OTCase viewed along a three-fold axis.

conserved in the other OTCase sequences. The role of such an unusual interface composed of positively charged residues located between three monomers and present at each edge of the dodecamer is still unknown; this region may likely be a potential binding site for the negatively charged allosteric activators, such as phosphate or nucleoside monophosphates. Preliminary crystallographic studies of complexes of the enzyme with various allosteric effectors indicate that the highly positively charged interfaces found between the trimers are involved in the binding of some positive allosteric effectors. These results and a detailed analysis of interfaces present in the dodecamer will be published elsewhere. A comparison between *E. coli* and *P. aeruginosa* OTCase structures will reveal the nature of all interfaces and the oligomerization processes, when the *E. coli* OTCase structure is available (30).

The quaternary structures of the catabolic OTCase and ATCase are quite different. In ATCase two catalytic trimers are present and aligned on the same threefold axis. These two trimers interact through the "240 loops" located on the concave faces of the trimers (29). Equivalent regions in OTCase have no apparent function and are oriented into the solvent. Three regulatory dimers are present in ATCase, which together with the catalytic trimers form a pseudo-32 point-group particle. These regulatory units are required for allosteric behavior: the holoenzyme can be easily dissociated by heat or mercurial compounds, resulting in active trimers with Michaelis–Menten kinetics (31). On the other hand, no regulatory chains are found in the allosteric catabolic OTCase. The dodecameric structure is very stable, and concentrations

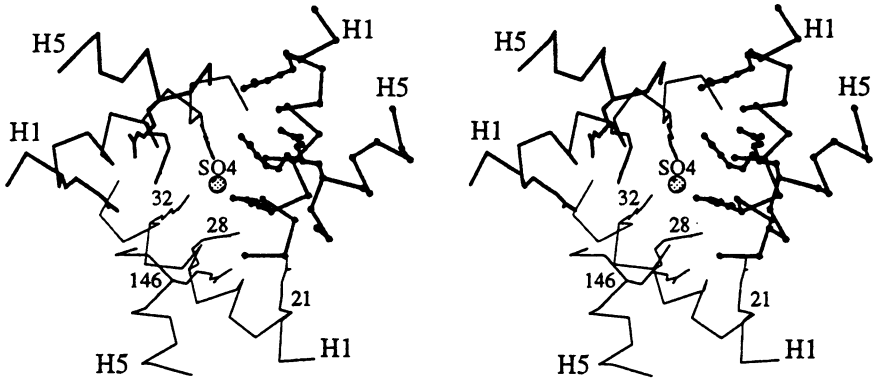

FIG. 4. Interface located around a threefold symmetry axis at the edge of the dodecamer. This interface involves helices H1 and H5 from three monomers belonging to three different trimers. Arginines at position 21, 28, 32, and 146 from each monomer are shown, with the α-carbons of the three H1 and H5 helices. The sulfate ion present on the threefold symmetry axis is represented as a sphere.

of at least 5 M urea are required to dissociate the particle. No activity is preserved after this treatment (unpublished data).

Active-Site Structure. The active sites are located between the polar and equatorial domains of each monomer, as identified in *E. coli* ATCase (32). Residues involved in the binding of carbamoyl phosphate in ATCase are also found in OTCase: this result could be expected from the high structural similarity found between the polar domains of the two enzymes. These residues are (in OTCase notation): Ser-56, Thr-57, Arg-58, Thr-59, Arg-107, and His-134. Quite interestingly, residue 105, present in the native OTCase as a glutamate and replaced by a glycine in the present structure, is found in strand B4, in the hydrophobic core of the carbamoyl phosphate domain. To compensate for this internal negative charge, Arg-107 might make a salt bridge with Glu-105 in the native enzyme. This arginine was shown to be critical for catalysis in both ATCases and OTCases (33, 34). Further studies are required to understand the exact role of Glu-105 in the allosteric regulation of the catabolic OTCase. Residues involved in the binding of aspartate in ATCase are not conserved in OTCase. The active site in the ornithine binding domain is probably defined by a tetrad (His-272, Cys-273, Leu-274, Pro-275), which is well conserved in all known OTCases, and by Asp-231 as suggested by a modeling study of the binding of the bisubstrate analogue *N*-phosphonoacetyl L-ornithine (PALO) into the active site. Cys-273 has been implicated in ornithine binding by chemical modification (35) and site-directed mutagenesis (19) on bovine and rat liver OTCases, respectively. Asp-231 is also conserved in all OTCase sequences and is a good candidate for making an electrostatic interaction with the α-amino group of ornithine. A crystallographic study of the enzyme complexed with this bisubstrate analogue is under way and will provide detailed information about the binding of substrates in the active site.

This is publication no. 282 of the Institut de Biologie Structurale Jean-Pierre Ebel. We thank D. Haas at the University of Lausanne for supplying the mutant protein gene; F. Vellieux at the LCCP/IBS Grenoble for useful discussions; and S. Marcq, P. Charlier, and M. Vermeire at the University of Liège for their help during preliminary crystallization and data collection trials. This work was supported by grants from the Belgian Fund for Joint Basic Research (no. 2.4507.91) and the French Ingénierie des Macromolécules Biologiques program. V.V. was supported by the Institut pour l'encouragement de la Recherche Scientifique dans l'Industrie et l'Agriculture (IRSIA), and V.S. is a Research Associate for Scientific Research (Belgium).

1. Stalon, V., Ramos, F., Piérard, A. & Wiame, J. M. (1967) *Biochim. Biophys. Acta* **139,** 91–97.
2. Haas, D., Evans, R., Mercenier, A., Simon, J. P. & Stalon, V. (1979) *J. Bacteriol.* **139,** 713–720.
3. Itoh, Y., Soldati, L., Stalon, V., Falmagne, P., Terawaki, Y., Leisinger, T. & Haas, D. (1988) *J. Bacteriol.* **170,** 3225–3234.
4. Stalon, V., Legrain, C. & Wiame, J. M. (1977) *Eur. J. Biochem.* **74,** 319–327.
5. Mercenier, A., Simon, J. P., Vander Wauven, C., Haas, D. & Stalon, V. (1980) *J. Bacteriol.* **144,** 159–163.
6. Vander Wauven, C., Piérard, A., Kley-Reymann, M. & Haas, D. (1984) *J. Bacteriol.* **160,** 928–934.
7. Baur, H., Tricot, C., Stalon, V. & Haas, D. (1990) *J. Biol. Chem.* **265,** 14728–14731.
8. Tricot, C., Nguyen, V. T. & Stalon, V. (1993) *Eur. J. Biochem.* **215,** 833–839.
9. Marcq, S., Diaz-Ruano, A., Charlier, P., Dideberg, O., Tricot, C., Piérard, N. & Stalon, V. (1991) *J. Mol. Biol.* **220,** 9–12.
10. Van Vliet, F., Cunin, R., Jacobs, A., Piette, J., Lauwereys, M., Piérard, A. & Glansdorff, N. (1984) *Nucleic Acids Res.* **12,** 6277–6289.
11. Haas, D., Baur, H., Tricot, C., Galimand, M. & Stalon, V. (1989) *Recent Advances in Microbial Ecology*, eds. Hattori, T., Ishida, Y., Maruyama, Y., Morita, R. Y. & Uchida, A. (Jpn. Sci. Soc. Press, Tokyo), pp. 617–619.
12. Lipscomb, W. N. (1994) *Adv. Enzymol. Relat. Areas Mol. Biol.* **68,** 67–151.
13. Messerschmidt, A. & Pflugrath, J. W. (1987) *J. Appl. Crystallogr.* **20,** 306–315.
14. Collaborative Computational Project, Number 4. The CCP4 Suite: Programs for Protein Crystallography (1994) *Acta Crystallogr.* **D50,** 760–763.
15. Matthews, B. W. (1968) *J. Mol. Biol.* **33,** 491–497.
16. Fitzgerald, P. M. D. (1988) *J. Appl. Crystallogr.* **21,** 273–278.
17. Brünger, A. T. (1992) X-PLOR: *A System for X-ray Crystallography and NMR* (Yale Univ. Press, New Haven, CT).
18. Tong, L. & Rossmann, M. G. (1990) *Acta Crystallogr.* **A46,** 783–792.
19. McDowall, S., van Heeswijck, R. & Hoogenraad, N. (1990) *Protein Eng.* **4,** 73–77.
20. Luo, M., Vriend, G., Kamer, G., Minor, I., Arnold, E., Rossmann, M. G., Boege, U., Scraba, D. G., Duke, G. M. & Palmenberg, A. C. (1987) *Science* **235,** 182–191.
21. Luo, M., Vriend, G., Kamer, G. & Rossmann, M. G. (1989) *Acta Crystallogr.* **B45,** 85–92.
22. Acharya, R., Fry, E., Stuart, D., Fox, G., Rowlands, D. & Brown, F. (1989) *Nature (London)* **337,** 709–716.
23. Navaza, J. (1993) *Acta Crystallogr.* **D49,** 588–591.
24. Vellieux, F. M. D. & Hol, W. G. J. (1989) *EMBO J.* **8,** 2171–2178.
25. Roussel, A. & Cambillau, C. (1989) *Silicon Graphics Geometry Partner Directory* (Silicon Graphics, Mountain View, CA), pp. 77–78.
26. Ke, H., Lipscomb, W. N., Cho, Y. & Honzatko, R. B. (1988) *J. Mol. Biol.* **204,** 725–747.
27. Krause, K. L., Volz, K. W. & Lipscomb, W. N. (1985) *Proc. Natl. Acad. Sci. USA* **82,** 1643–1647.
28. Krause, K. L., Volz, K. W. & Lipscomb, W. N. (1987) *J. Mol. Biol.* **193,** 527–553.
29. Stevens, R. C., Chook, Y. M., Cho, Y. O., Lipscomb, W. N. & Kantrowitz, E. R. (1991) *Protein Eng.* **4,** 391–408.
30. Kuo, L. C. & Seaton, B. A. (1989) *J. Biol. Chem.* **264,** 16246–16248.
31. Hunt, J. B., Neece, S. H., Schachman, H. K. & Ginsburg, A. (1984) *J. Biol. Chem.* **259,** 14793–14803.
32. Monaco, H. L., Crawford, J. L. & Lipscomb, W. N. (1978) *Proc. Natl. Acad. Sci. USA* **75,** 5276–5280.
33. Stebbins, J. W., Xu, W. & Kantrowitz, E. R. (1989) *Biochemistry* **28,** 2592–2600.
34. Kuo, L. C., Zambidis, I. & Caron, C. (1989) *Science* **245,** 522–524.
35. Marshall, M. & Cohen, P. P. (1980) *J. Biol. Chem.* **255,** 7296–7300.